Journal of Statistical Physics, Vol. 107, Nos. 1/2, April 2002 (© 2002)

A New Differential Lattice Boltzmann Equation and Its Application to Simulate Incompressible Flows on Non-Uniform Grids

Y. T. Chew,[1] C. Shu,[1] and X. D. Niu[1]

Received February 14, 2001; accepted October 15, 2001

A new differential lattice Boltzmann equation (LBE) is presented in this work, which is derived from the standard LBE by using Taylor series expansion only in spatial direction with truncation to the second-order derivatives. The obtained differential equation is not a wave-like equation. When a uniform grid is used, the new differential LBE can be exactly reduced to the standard LBE. The new differential LBE can be applied to solve irregular problems with the help of coordinate transformation. The present scheme inherits the merits of the standard LBE. The 2-D driven cavity flow is chosen as a test case to validate the present method. Favorable results are obtained and indicate that the present scheme has good prospects in practical applications.

KEY WORDS: Taylor series expansion; lattice Boltzmann equation; differential equation; incompressible flow.

1. INTRODUCTION

There has been a rapid progress in developing and employing the lattice Boltzmann equation (LBE) as an alternative computational fluid dynamics approach for simulation of complex flows.[1–6] However, because of the essential restriction of the standard LBE to the uniformity of lattice,[6] the broad application of LBE in engineering has been greatly hampered. For many practical problems, an irregular grid is always preferable due to

[1] Department of Mechanical Engineering, National University of Singapore, 10 Kent Ridge Crescent, Singapore 119260; e-mail: mpeshuc@nus.edu.sg

0022-4715/02/0400-0329/0 © 2002 Plenum Publishing Corporation

the fact that curved boundaries can be described more accurately, and computational resources can be used more efficiently with it.

The lattice-uniformity requirement of the standard LBE comes from its precursor, the lattice-gas automata (LGA) method.[2] In the LGA, all the particles have the same mass, and a particle at one grid point must move to its neighboring point in one time step. This requirement leads to the lattice-uniformity. Lattice Boltzmann method (LBM) is developed from the LGA, in which the mass of particle is replaced by the density distribution function. In general, the collision operator is linearized by BGK approximation[7] in the LBM. The LBM enhances the computational efficiency of the LGA method but inherits its feature of the lattice-uniformity. Theoretically, this feature is not necessary to be kept because the distribution functions are continuous in physical space.[8]

Currently, there are three ways to improve the standard LBE so that it can be applied to complex problems.[9–18] The first is the interpolation-supplemented LBE (ISLBE) proposed by He and his colleagues.[9–11] In this method, interpolation is applied at every time step in order to obtain the density distribution function at the grid point. So, the computational effort by this method is very large as compared to the standard LBM. The second is based on the solution of a partial differential equation. For simplicity, this scheme is called the differential LBE. For complex problems, the differential LBE can be solved by conventional finite difference schemes with the use of coordinate transformation[16] or by finite volume method.[12–15] The third is the grid refine technique which was first presented by Fillipova and Hänel[17] in 1998 and further improved by Mei *et al.*[18] This technique is based on the conventional adaptive mesh refinement method, using a coarse grid in the whole domain and a finer grid in critical regions. Second order interpolation is used on the interfaces and boundaries of different grid levels. All these schemes have shown good accuracy in their applications.

In this work, we will present a new differential LBE, which is derived from the standard LBE. In our model, the Taylor series expansion is only applied in the space direction and the second order derivatives are included in the expansion. As a consequence, the resultant differential equation only contains the spatial derivatives and is no longer a wave-like equation. For complex problems or non-uniform grids, the obtained differential equation is transformed into the form in the curvilinear coordinate system, where the numerical computation is conducted. Our new differential model can be exactly reduced to the standard LBE when uniform lattices are used. It was found that when our model is applied to simulate the driven cavity flow, very accurate results could be obtained, which are much better than those obtained by the conventional differential LBE.

2. STANDARD LBE AND CONVENTIONAL DIFFERENTIAL LBE

The two dimensional, standard LBE with BGK approximation can be written as

$$f_\alpha(x+e_{\alpha x}\,\delta t,\, y+e_{\alpha y}\,\delta t,\, t+\delta t) = f_\alpha(x, y, t)+[f_\alpha^{eq}(x, y, t)-f_\alpha(x, y, t)]/\tau \quad \text{for } \alpha=0, 1, 2,..., 8 \tag{1}$$

where τ is the single relaxation parameter,[5] f_α is the density distribution function, f_α^{eq} is its corresponding equilibrium state, δ_t is the time step and e_α is the particle velocity in the α direction. The nine discrete velocities $\mathbf{e}_\alpha = (e_{\alpha x}, e_{\alpha y})$ are defined as

$$\mathbf{e}_\alpha = \begin{cases} (0, 0), & \alpha=0 \\ (\cos[(\alpha-1)\,\pi/2], \sin[(\alpha-1)\,\pi/2]), & \alpha=1,..., 4 \\ (\cos[(\alpha-5)\,\pi/2+\pi/4], \sin[(\alpha-5)\,\pi/2+\pi/4])\,\sqrt{2}, & \alpha=5,..., 8 \end{cases} \tag{2}$$

The equilibrium density distribution function f_α^{eq} is chosen to be in ref. 5

$$f_\alpha^{eq} = w_\alpha\rho[1+3(e_{ax}u+e_{ay}v)+\tfrac{9}{2}(e_{ax}u+e_{ay}v)^2-\tfrac{3}{2}(u^2+v^2)] \tag{3}$$

with $w_0=4/9$, $w_\alpha=1/9$ for $\alpha=1,..., 4$, and $w_\alpha=1/36$ for $\alpha=5,..., 8$. The macroscopic density ρ, the velocity u and v are obtained from

$$\sum_\alpha f_\alpha = \rho\sum_\alpha f_\alpha e_{\alpha x} = \rho u \qquad \text{and} \qquad \sum_\alpha f_\alpha e_{\alpha y} = \rho v \tag{4}$$

The speed of sound of this model is $c_s = 1/\sqrt{3}$, and pressure can be directly computed from the equation of state

$$P = \rho c_s^2 \tag{5}$$

The lattice-uniformity of the standard LBE (1) requires that $\delta x = e_{\alpha x}\cdot\delta_t$, $\delta y = e_{\alpha y}\cdot\delta_t$. This feature is quite restrictive in many applications involving external flows where a large gradient exists only in a small region while the domain of interest is large. To improve the standard LBE for its general application, the differential LBE can be developed by using the Taylor series expansion. Using the following Taylor series expansion

$$f_\alpha(x+e_{\alpha x}\delta_t,\, y+e_{\alpha y}\delta_t,\, t+\delta_t) = f_\alpha(x, y, t)+e_{\alpha x}\delta_t\frac{\partial f_\alpha(x, y, t)}{\partial x}+e_{\alpha y}\delta_t\frac{\partial f_\alpha(x, y, t)}{\partial y}+\delta_t\frac{\partial f_\alpha(x, y, t)}{\partial t}+O(\delta_t^2) \tag{6}$$

Equation (1) can be reduced to

$$\frac{\partial f_\alpha(x, y, t)}{\partial t} + e_{\alpha x}\frac{\partial f_\alpha(x, y, t)}{\partial x} + e_{\alpha y}\frac{\partial f_\alpha(x, y, t)}{\partial y}$$

$$= [f_\alpha^{eq}(x, y, t) - f_\alpha(x, y, t)]/(\tau\delta_t) \tag{7}$$

Equation (7) is a wave-like differential equation, which has the same form as the discrete Boltzmann equation. From the process of derivation, we can see that Eq. (7) is the result of the first-order Taylor series expansion of Eq. (1) in time and space. Even when uniform lattices ($\delta x = e_{\alpha x}\cdot\delta_t$, $\delta y = e_{\alpha y}\cdot\delta_t$) are used, Eq. (7) may not be reduced to Eq. (1). Due to these factors, Eq. (7) may not be able to give accurate results for some problems. An example is the simulation of 2-D driven cavity flow by using the FD method to solve Eq. (7). Even on very fine uniform mesh, the obtained results are still not accurate. It seems that the improvement of Eq. (7) is to include the second order derivative terms in the Taylor series expansion. As will be shown in Section 5, when our model with inclusion of the second order derivatives is applied to simulate the driven cavity flow, very accurate results can be obtained on the uniform and non-uniform meshes.

3. A NEW DIFFERENTIAL LBE

In this section, a new differential LBE is presented. The idea is that the Taylor series expansion is only applied for Eq. (1) in the spatial direction and the second order derivatives are included in the expansion. Suppose that a particle is initially at the grid point (x, y) at a time level t. Along the α direction, this particle will move to the position $(x+e_{\alpha x}\delta_t, y+e_{\alpha y}\delta_t)$ at its next time level $t+\delta_t$. For complex problems or non-uniform meshes, the position $(x+e_{\alpha x}\delta_t, y+e_{\alpha y}\delta_t)$ is usually not at the grid point $(x+\delta x, y+\delta y)$. To get the density distribution function at the grid point $(x+\delta x, y+\delta y)$ and the time level $t+\delta_t$, we need to apply the Taylor series expansion or other interpolation techniques such as the one used by He *et al.*[9–11] In this work, the Taylor series expansion is used. Note that the time level for the position $(x+e_{\alpha x}\delta_t, y+e_{\alpha y}\delta_t)$ and the grid point $(x+\delta x, y+\delta y)$ is the same, that is, $t+\delta_t$. So, the expansion in the time direction is not necessary. Using the function value and its derivatives at the grid point $(x+\delta x, y+\delta y)$, $f_\alpha(x+e_{\alpha x}\delta_t, y+e_{\alpha y}\delta_t, t+\delta_t)$ can be approximated by

$$
\begin{aligned}
& f_\alpha(x+e_{\alpha x}\delta_t,\, y+e_{\alpha y}\delta_t,\, t+\delta_t) \\
&\quad = f_\alpha(x+\delta x,\, y+\delta y,\, t+\delta_t)+(e_{\alpha x}\delta_t-\delta x)\frac{\partial f_\alpha(x+\delta x,\, y+\delta y,\, t+\delta_t)}{\partial x} \\
&\qquad +(e_{\alpha y}\delta_t-\delta y)\frac{\partial f_\alpha(x+\delta x,\, y+\delta y,\, t+\delta_t)}{\partial y} \\
&\qquad +\frac{1}{2}(e_{\alpha x}\delta_t-\delta x)^2\frac{\partial^2 f_\alpha(x+\delta x,\, y+\delta y,\, t+\delta_t)}{\partial x^2} \\
&\qquad +\frac{1}{2}(e_{\alpha y}\delta_t-\delta y)^2\frac{\partial^2 f_\alpha(x+\delta x,\, y+\delta y,\, t+\delta_t)}{\partial y^2} \\
&\qquad +(e_{\alpha x}\delta_t-\delta x)(e_{\alpha y}\delta_t-\delta y)\frac{\partial^2 f_\alpha(x+\delta x,\, y+\delta y,\, t+\delta_t)}{\partial x\,\partial y} \\
&\qquad +O[(e_{\alpha x}\delta_t-\delta x)^3,\,(e_{\alpha y}\delta_t-\delta y)^3] \qquad (8)
\end{aligned}
$$

Now, substituting Eq. (8) into Eq. (1) leads to

$$
\begin{aligned}
& f_\alpha(x+\delta x,\, y+\delta y,\, t+\delta_t)+(e_{\alpha x}\delta_t-\delta x)\frac{\partial f_\alpha(x+\delta x,\, y+\delta y,\, t+\delta_t)}{\partial x} \\
&\qquad +(e_{\alpha y}\delta_t-\delta y)\frac{\partial f_\alpha(x+\delta x,\, y+\delta y,\, t+\delta_t)}{\partial y} \\
&\qquad +\frac{1}{2}(e_{\alpha x}\delta_t-\delta x)^2\frac{\partial^2 f_\alpha(x+\delta x,\, y+\delta y,\, t+\delta_t)}{\partial x^2} \\
&\qquad +\frac{1}{2}(e_{\alpha y}\delta_t-\delta y)^2\frac{\partial^2 f_\alpha(x+\delta x,\, y+\delta y,\, t+\delta_t)}{\partial y^2} \\
&\qquad +(e_{\alpha x}\delta_t-\delta x)(e_{\alpha y}\delta_t-\delta y)\frac{\partial^2 f_\alpha(x+\delta x,\, y+\delta y,\, t+\delta_t)}{\partial x\,\partial y} \\
&\quad = f_\alpha(x,\, y,\, t)+[f_\alpha^{eq}(x,\, y,\, t)-f_\alpha(x,\, y,\, t)]/\tau \qquad (9)
\end{aligned}
$$

Note that all the spatial derivatives in Eq. (9) are evaluated at the time level $t+\delta_t$. It is interesting to notice that when uniform lattices are used, that is, $\delta x = e_{\alpha x}\cdot\delta_t$, $\delta y = e_{\alpha y}\cdot\delta_t$, Eq. (9) can be exactly reduced to Eq. (1). As compared to Eqs. (7) and (9) involves the second order derivatives. For some problems with curved boundaries, Eq. (9) can be applied with the

help of coordinate transformation. In such cases, the irregular physical domain in the Cartesian coordinate system can be mapped to a regular domain in the general coordinate system by the following equation

$$\begin{cases} x = x(\xi, \eta) \\ y = y(\xi, \eta) \end{cases} \tag{10}$$

With Eq. (10), and Eq. (9) can be transformed into the following form

$$\begin{aligned} & f_\alpha(\xi+\delta\xi, \eta+\delta\eta, t+\delta_t) + A\frac{\partial f_\alpha(\xi+\delta\xi, \eta+\delta\eta, t+\delta_t)}{\partial\xi} \\ & \quad + B\frac{\partial f_\alpha(\xi+\delta\xi, \eta+\delta\eta, t+\delta_t)}{\partial\eta} + C\frac{\partial^2 f_\alpha(\xi+\delta\xi, \eta+\delta\eta, t+\delta_t)}{\partial\xi^2} \\ & \quad + D\frac{\partial^2 f_\alpha(\xi+\delta\xi, \eta+\delta\eta, t+\delta_t)}{\partial\eta^2} + E\frac{\partial^2 f_\alpha(\xi+\delta\xi, \eta+\delta\eta, t+\delta_t)}{\partial\xi\,\partial\eta} \\ & = f_\alpha(\xi, \eta, t) + [f_\alpha^{eq}(\xi, \eta, t) - f_\alpha(\xi, \eta, t)]/\tau \end{aligned} \tag{11}$$

The coefficients A, B, C, D, and E in Eq. (11) are

$$\mathbf{A} = \alpha + \tfrac{1}{2}\alpha^2\mathbf{J}_{\eta\varsigma\xi} + \alpha\beta\mathbf{J}_{\eta\varsigma\eta} + \tfrac{1}{2}\beta^2\mathbf{J}_{\eta\eta\eta}$$

$$\mathbf{B} = \beta + \frac{1}{2}\alpha^2\mathbf{J}_{\xi\varsigma\xi} + \alpha\beta\mathbf{J}_{\xi\varsigma\eta} + \tfrac{1}{2}\beta^2\mathbf{J}_{\xi\eta\eta}$$

$$\mathbf{C} = \tfrac{1}{2}\alpha^2 \quad \mathbf{D} = \tfrac{1}{2}\beta^2 \quad \mathbf{E} = \alpha\beta$$

where

$$\alpha = [(\mathbf{e}_{\alpha x}\delta_t - \Delta\mathbf{x})\,\mathbf{y}_\eta - (\mathbf{e}_{\alpha y}\delta_t - \Delta\mathbf{y})\,\mathbf{x}_\eta]/\mathbf{J},$$

$$\beta = [-(\mathbf{e}_{\alpha x}\delta_t - \Delta\mathbf{x})\,\mathbf{y}_\xi + (\mathbf{e}_{\alpha y}\delta_t - \Delta\mathbf{y})\,\mathbf{x}_\xi]/\mathbf{J},$$

$$\mathbf{J} = \mathbf{x}_\xi\,\mathbf{y}_\eta - \mathbf{x}_\eta\,\mathbf{y}_\xi, \qquad \mathbf{J}_{\eta\xi\xi} = (\mathbf{x}_\eta\,\mathbf{y}_{\xi\xi} - \mathbf{x}_{\xi\xi}\,\mathbf{y}_\eta)/\mathbf{J},$$

$$\mathbf{J}_{\eta\eta\eta} = (\mathbf{x}_\eta\,\mathbf{y}_{\eta\eta} - \mathbf{x}_{\eta\eta}\,\mathbf{y}_\eta)/\mathbf{J}, \qquad \mathbf{J}_{\xi\xi\xi} = -(\mathbf{x}_\xi\,\mathbf{y}_{\xi\xi} - \mathbf{x}_{\xi\xi}\,\mathbf{y}_\xi)/\mathbf{J},$$

$$\mathbf{J}_{\xi\xi\eta} = -(\mathbf{x}_\xi\,\mathbf{y}_{\xi\eta} - \mathbf{x}_{\xi\eta}\,\mathbf{y}_\xi)/\mathbf{J}, \qquad \mathbf{J}_{\eta\xi\eta} = -(\mathbf{x}_\xi\,\mathbf{y}_{\eta\eta} - \mathbf{x}_{\eta\eta}\,\mathbf{y}_\xi)/\mathbf{J}$$

It is indicated that Eq. (10) can also be used to transform a non-uniform mesh in the (x, y) plane to the uniform mesh in the (ξ, η) plane. Then Eq. (11) is solved on the uniform mesh in the (ξ, η) plane. It is noted that both Eqs. (9) and (11) are implicit forms. After numerical discretization, they can be solved by iterative methods such as SOR approach.

4. NUMERICAL IMPLEMENTATION

4.1. Finite Difference Discretization of New Differential LBE

Unlike the standard LBE, Eqs. (9) or (11) is a partial differential equation, which has to be solved by a numerical method. In this work, we will apply the finite difference scheme to do numerical discretization.

It was found that the central difference discretization of Eqs. (9) or (11) could provide the stable solution. However, since the convection is dominated in the LBE model, a second order upwind difference discretization to the first-order derivatives can greatly enhance the stability of numerical computation. Therefore, in this work, the first order derivatives are approximated by the second-order upwind scheme. For example, $\partial f_\alpha / \partial \xi$ is approximated by

$$\begin{aligned} \frac{\partial f_\alpha}{\partial \xi} &= \frac{3f_{\alpha i,j} - 4f_{\alpha i-1,j} + f_{\alpha i-2,j}}{2\Delta\xi}, \qquad \text{when} \quad A \geqslant 0 \\ &= \frac{-3f_{\alpha i,j} + 4f_{\alpha i+1,j} - f_{\alpha i+2,j}}{2\Delta\xi}, \qquad \text{when} \quad A < 0 \end{aligned} \tag{12}$$

where i and j are indexes of the grid point in the ξ- and η-directions, respectively. For discretization of the second-order derivatives, both the second order central and upwind difference schemes can be employed, but the central difference scheme is easier to implement. The discretization of $\partial^2 f_\alpha / \partial \xi^2$ can be made by

$$\left.\frac{\partial^2 f_\alpha}{\partial \xi^2}\right|_{\text{central}} = \frac{f_{\alpha i+1,j} - 2f_{\alpha i,j} + f_{\alpha i-1,j}}{\Delta\xi^2} \tag{13}$$

and

$$\begin{aligned} \left.\frac{\partial^2 f_\alpha}{\partial \xi^2}\right|_{\text{upwind}} &= \frac{2f_{\alpha i,j} - 5f_{\alpha i-1,j} + 4f_{\alpha i-2,j} - f_{\alpha i-3,j}}{\Delta\xi^2}, \qquad \text{when} \quad C \geqslant 0 \\ &= \frac{2f_{\alpha i,j} - 5f_{\alpha i+1,j} + 4f_{\alpha i+2,j} - f_{\alpha i+3,j}}{\Delta\xi^2}, \qquad \text{when} \quad C < 0 \end{aligned} \tag{14}$$

The discretization of derivatives in the η direction can be done in a similar way. It should be indicated that when Eq. (7) (the conventional differential LBE) is solved, the same second-order upwind schemes like Eq. (12) are applied for numerical discretization. So, in this work, the

numerical discretization of the conventional differential LBE and the new differential LBE has the same order of truncation error, which is the second order.

4.2. Bounce Back Condition on a Solid Wall

Numerical computation of Eq. (11) needs to implement the boundary condition on the solid wall. So far, there are several ways to implement the boundary conditions.[17–28] Among them, the bounce back condition is the simplest one. On the wall, the density distribution functions in the outward direction from the flow field are computed from the solution of Eq. (11), while the density distribution functions in the inward direction to the flow field are determined by the boundary condition. For 9-bits lattice model[5] used in this work, the bounce back condition gives $f_{\alpha'} = f_{\alpha}$, where $\mathbf{e}_{\alpha'} = -\mathbf{e}_{\alpha}$, α is the outward direction from the flow field and α' is the inward direction to the flow field.

5. NUMERICAL RESULTS AND DISCUSSION

The new differential LBE outlined above is now applied to simulate one simple, yet nontrivial flow—the flow in a 2-D lid driven cavity. It is noted that the above case has singularities at corners, which need be treated carefully.

5.1. Flow in a 2-D Lid Driven Cavity

For this problem, the top boundary moves from left to right with a constant velocity U while other boundaries are stationary. The present simulation directly solves Eq. (11) in the (ξ, η) plane. Initially a constant density, $\rho_0 = 1.0$, is prescribed in the whole field, and the velocities in the interior of the cavity are set to zero. On the top, the x-direction velocity is U and the y-direction velocity is zero. On the top (moving) boundary, two types of boundary conditions are implemented to test their accuracy. One is the equilibrium distribution function boundary condition (EDFBC),[27] and the other is the hydrodynamic boundary condition (HBC),[28] in which the unknown distribution functions on the boundary are computed from the solution of Eq. (4) (mass and momentum conservation). The bounce back boundary condition is applied on other three boundaries. It was found that, the two upper corners, which are singular points, can be treated as stationary points (with zero velocity) or moving points (with velocity U). Very little difference of these two cases was found in our simulation. The

Mach number is chosen as $\mathrm{Ma} = 0.15$, so the velocity of the top wall can be calculated by $U = \mathrm{Ma} \cdot c_s$. The Reynolds number used in the simulation is defined as $\mathrm{Re} = UL/v$, where L is the characteristic length set as the value of top wall, and v is the kinematic viscosity.

The driven cavity flow is a standard test case, which has been studied by many researchers. Ghia *et al.*[29] gave a detailed study for this problem by using the multi-grid finite difference scheme to solve the vorticity-stream function formulation. Hou *et al.*[27] also gave detailed results for $\mathrm{Re} = 100 \sim 10{,}000$ on a uniform 256×256 lattice by using the standard LBE. Thus, their results are taken as benchmark solutions to validate our results and test our new algorithm. In our simulation, the case of $\mathrm{Re} = 400$ is presented at different mesh sizes. All the results are normalized to simplify our comparison between the present algorithm on a non-uniform grid, the standard LBE on a uniform grid, the conventional differential LBE on a non-uniform grid.

It is indicated that in the present work, both the conventional differential LBE and the new differential LBE are discretized by the second order finite difference schemes.

5.2. Results of Conventional Differential LBE

The conventional differential LBE is firstly applied to solve this problem. It was found that even using a uniform lattice, the obtained numerical results are not accurate as compared to those of Ghia *et al.*[29] and of the standard LBE. This can be observed clearly from Fig. 1, which shows the velocity profiles along the vertical and horizontal centerlines. Shown in Fig. 1 are the results of conventional differential LBE (noted as

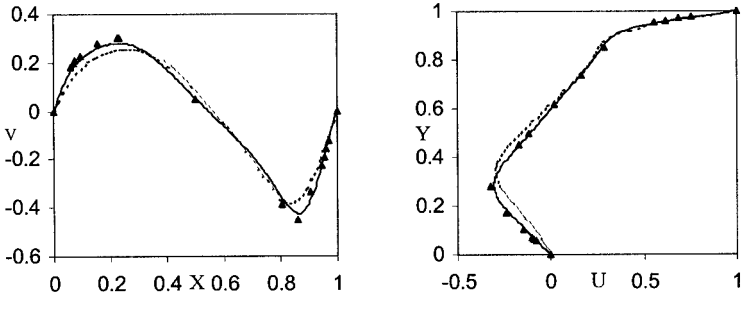

Fig. 1. Velocity profiles along horizontal and vertical centerlines with $\mathrm{Re} = 400$ (— the standard LBE with EDFBC (65×65); ---- the CDLBE with EDFBC(65(85); ▲ (Ghia's result).

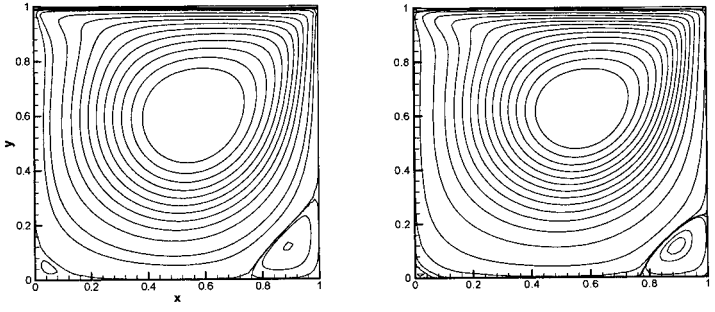

(a) Standard LBE with EDFBC(65×65); (b) CDLBE with EDFBC(65×85)

Fig. 2. Streamlines of Re = 400 obtained by standard LBE and CDLBE.

CDLBE in the figure for simplicity), the standard LBE, and Ghia *et al.*[29] Note that the standard LBE is based on a uniform mesh of 65×65 while the conventional differential LBE is based on a mesh of 65×85, and both methods adopt equilibrium distribution function boundary condition on the moving boundary. From Fig. 1, we can see that the velocity profiles obtained by the CDLBE have obvious deviations from those of the standard LBE and Ghia *et al.*[29] The vortex positions obtained by the conventional differential LBE and the standard LBE are also different. This can be seen from Fig. 2 and Table I. Fig. 2 shows the streamlines of two methods while Table I gives the detailed numerical comparison for the vortex positions. All these comparisons show that the conventional differential LBE cannot give a satisfactory result for this problem.

To reduce the effect of the boundary conditions, the hydrodynamic boundary condition,[28] which has been viewed as a more accurate treatment for the moving boundaries, is also used for the conventional differential LBE and the standard LBE. Figure 3 shows the velocity profiles along the vertical and horizontal centerlines obtained by these two methods. Obvious difference between the two results can also be observed.

Table I. Vortex Positions Obtained by Conventional Differential LBE (CDLBE), the Standard LBE, and Ghia *et al.*[29]

Method	Main vortex	Right second vortex	Left second vortex
Ghia *et al.*[29]	(0.56, 0.61)	(0.88, 0.12)	(0.047, 0.046)
Standard LBE (EDFBC)	(0.559, 0.608)	(0.893, 0.117)	(0.047, 0.046)
CDLBE (EDFCB)	(0.562, 0.625)	(0.89, 0.109)	(0.0156,0.0155)

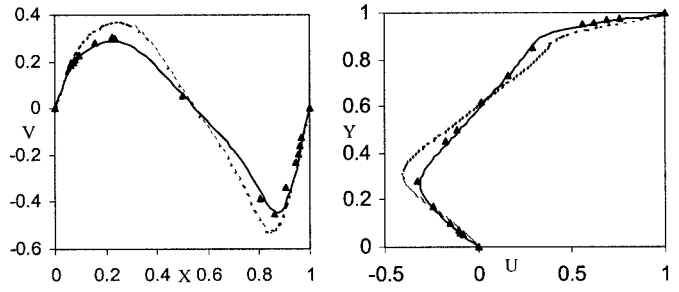

Fig. 3. Velocity profiles along horizontal and vertical centerlines with Re = 400 (— the standard LBE with HBC (65 × 65); ---- the CDLBE with HBC(65 × 85); ▲ (Ghia's result).

5.3. Results of New Differential LBE

The new differential LBE developed in this work has considered the second-order diffusion terms. Thus, it is expected to give better results as compared to the conventional differential LBE. This is confirmed in Figs. 4 and 5, which show the velocity profiles along the vertical and horizontal centerlines obtained by the new differential LBE with central and upwind difference discretization, the standard LBE, and Ghia *et al.*[29] The standard LBE is still based on a uniform mesh of 65 × 65, and like the conventional differential LBE, the new differential LBE is based on a mesh of 65 × 85. The results in Figs. 4 and 5 are based on the equilibrium distribution and hydrodynamic boundary conditions, respectively. From Figs. 4 and 5, it can be seen that the present results agree very well with those of the standard LBE and Ghia *et al.*[29] In Fig. 4, the central difference and the upwind difference discretization of new differential LBE shows no

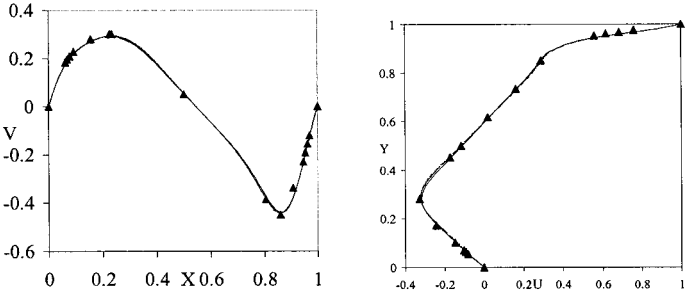

Fig. 4. Velocity profiles along horizontal and vertical central lines with Re = 400 (— the standard LBE with EDFBC (65 × 65); — - - — the new differential LBE with upwind difference and EDFBC (65 × 85); — - - - — the new differential LBE with central difference and EDFBC (65 × 85); ▲ (Ghia's result).

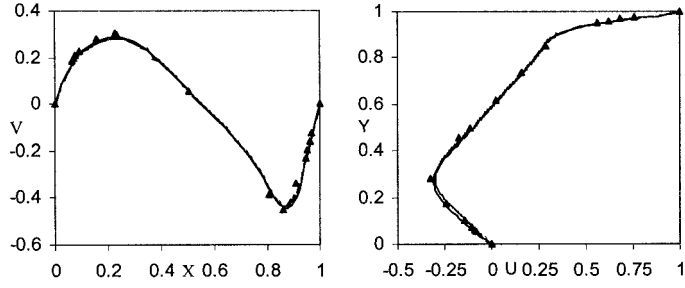

Fig. 5. Velocity profiles along horizontal and vertical central lines with Re = 400 (— the standard LBE with HBC (65 × 65); — - — the new differential LBE with central difference and HBC (65 × 85); ▲ (Ghia's result).

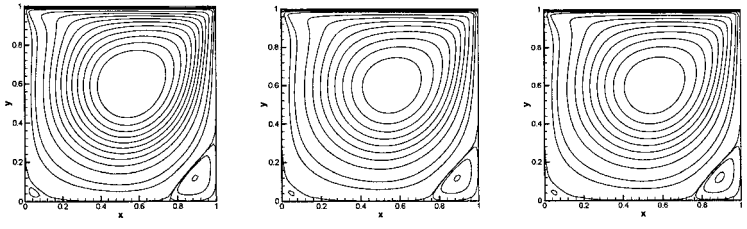

(a) standard LBE (65×65) with EDFBC

(b) present method with upwind difference and EDFBC (65×85)

(c) present method with central difference with EDFBC (65×85)

Fig. 6. Streamlines of Re = 400 obtained by standard LBE and present method.

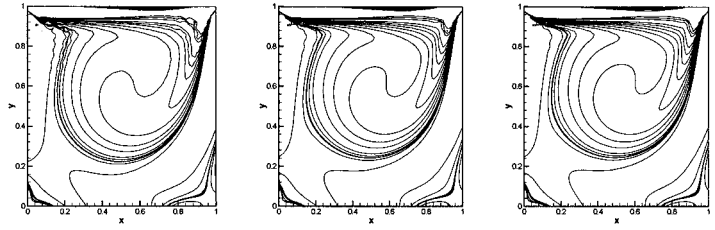

(a) standard LBE (65×65) with EDFBC

(b) present method with upwind difference and EDFBC (65×85)

(c) present method with central difference with EDFBC (65×85)

Fig. 7. Contours of vorticity for Re = 400 obtained by standard LBE and present method.

deviation in the numerical results. It can be seen from Fig. 5 that , under the treatment of the hydrodynamic boundary condition on the moving boundary, the results obtained from our new differential LBE, the standard LBE and Ghia *et al.*[29] agree very well, and no much difference was found when compared with the results by using the equilibrium distribution condition on the moving boundary. The streamlines and vorticity contours of the standard LBE, the new differential LBE with central and upwind difference discretization are shown respectively in Figs. 6 and 7. Clearly, these results agree very well with each other, which also have a good agreement with those of Ghia *et al.*[29] In addition, the vortex positions obtained by our new method coincide with those of the standard LBE and Ghia *et al.*[29] From this example, we can say that the present differential LBE is able to provide accurate numerical results.

6. CONCLUSIONS

A new differential lattice Boltzmann equation was developed in this work, which was successfully applied to simulate the 2-D driven cavity flow on non-uniform grids. The results obtained by present model are in good agreement with those of the standard LBE and available data in the literature. It is indicated that the new differential equation is not a wave-like equation. As compared with the conventional differential LBE, the present model gives more accurate results for the simulation of driven cavity flow. For the comparison with the standard LBE, it can provide the same order of accuracy but require more computational effort. The major advantage of present model over the standard LBE is that it can be applied to problems with complex geometry.

ACKNOWLEDGMENTS

The authors would like to thank Dr. He Xiaoyi and Professor Mei Renwei for their helpful discussion during this work.

REFERENCES

1. J. Hardy, O. de Pazzis, and Y. Pomeau, *Phys. Rev. A* **13**:1949 (1976).
2. U. Frisch, B. Hasslacher, and Y. Pomeau , *Phys. Rev. Lett.* **56**:1505 (1986).
3. G. R. McNamara and G. Zanetti, *Phys. Rev. Lett.* **61**:2332 (1988).
4. F. J. Higuera, S. Succi, and R. Benzi, *Europhys. Lett.* **9**:345 (1989).
5. Y. H. Qian, Ph.D. thesis (Université Pierre et Marie Curie, Paris, 1990).
6. H. Chen, S. Chen, and W. H. Matthaeus, *Phys. Rev. A* **45**:R5339 (1992).
7. P. L. Bhatnagar, E. P. Gross, and M. Krook, *Phys.Rev. Lett.* **94**:511 (1954).

8. N. Cao, S. Chen, S. Jin, and D. Martinez, *Phys. Rev. E* **55**:R21 (1997).
9. X. He, L-S. Luo, and M. Dembo, *J. Comput. Phys.* **129**:357 (1996).
10. X. He, L-S. Luo, and M. Dembo, *J. Stat. Phys.* **87**:115 (1997).
11. X. He and G. D. Doolen, *Phys. Rev. E* **56**:434 (1997).
12. S. Succi, G. Amati, and R. Benzi, *J. Stat. Phys.* **81**:5 (1995).
13. F. Nannelli and S. Succi, *J. Stat. Phys.* **68**:401 (1992).
14. G. Peng, H. Xi, C. Duncan, and S.-H. Chou, *Phys. Rev. E* **58**:R4124 (1998).
15. G. Peng, H. Xi, and C. Duncan, *Phys. Rev. E* **59**:4675 (1999).
16. R. Mei and W. Shyy, *J. Comput. Phys.* **143**:426 (1998).
17. O. Filippova and D. Hänel, *J. Comp. Phys.* **147**:219 (1998).
18. R. Mei, L.-S. Luo, and W. Shyy, *J. Comp. Phys.* **155**:307 (1999).
19. S. Chen and G. D. Doolen, Lattice Boltzmann method for fluid flows, *Annu. Rev. Fluid Mech.* **30**:329 (1998).
20. X. He and L.-S. Luo, *Phys. Rev. E* **55**:6333 (1997).
21. S. Wolfram, *J. Stat. Phys.* **45**:471 (1986).
22. P. A. Skordos, *Phys. Rev. E* **48**:4823 (1993).
23. D. R. Nobel, S. Chen, J. G. Georgiadis, and R. O. Buckius, *Phys. Fluids* **7**:203 (1995).
24. Q. Zou and X. He, *Phys. Fluids* **9**:1591 (1997).
25. D. P. Ziegler, *J. Stat. Phys.* **71**:1171 (1993).
26. S. Chen, D. Martinez, and R. Mei, *Phys. Fluids* **8**:2527 (1996).
27. S. Hou, Q. Zou, S. Chen, G. D. Doolen, and A. C. Cogley, *J. Comput. Phys.* **118**:329 (1995).
28. D. R. Noble, J. G. Georgiadis, and R. O. Buckius, *J. Stat. Phys.* **81**:17 (1005).
29. U. Ghia, K. N. Ghia, and H. B. Keller, *J. Comput. Phys.* **48**:387 (1982).